BIOCHEMISTRY
including biophysical chemistry & molecular biology
Article

Biochemistry **XXXX,** *XXX,* 000–000 A
DOI: 10.1021/bi901338d

Characterization of a Signaling Complex Composed of Sensory Rhodopsin I and Its Cognate Transducer Protein from the Eubacterium *Salinibacter ruber*†

Yuki Sudo,*,‡,§,@ Akiko Okada,‡,@ Daisuke Suzuki,‡ Keiichi Inoue,∥ Hiroki Irieda,‡ Makoto Sakai,∥ Masaaki Fujii,∥ Yuji Furutani,⊥ Hideki Kandori,⊥ and Michio Homma‡

‡*Division of Biological Science, Graduate School of Science, Nagoya University, Chikusa-ku, Nagoya 464-8602, Japan,* §*PRESTO, Japan Science and Technology Agency (JST), 4-1-8 Honcho Kawaguchi, Saitama 332-0012, Japan,* ∥*Chemical Resources Laboratory, Tokyo Institute of Technology, 4259 Nagatsuta-cho, Midori-ku, Yokohama 226-8503, Japan, and* ⊥*Department of Frontier Materials, Nagoya Institute of Technology, Showa-ku, Nagoya 466-8555, Japan* @*These authors equally contributed to this work.*

Received August 3, 2009; Revised Manuscript Received September 23, 2009

ABSTRACT: Sensory rhodopsin I (SRI) exists in the cell membranes of microorganisms such as the archaeon *Halobacterium salinarum* and is a photosensor responsible for positive and negative phototaxis. SRI forms a signaling complex with its cognate transducer protein, HtrI, in the membrane. That complex transmits light signals to the flagellar motor through changes in protein−protein interactions with the kinase CheA and the adaptor protein CheW, which controls the direction of the rotation of the flagellar motor. Recently, we cloned and characterized *Salinibacter* sensory rhodopsin I (*Sr*SRI), which is the first SRI-like protein identified in eubacteria [Kitajima-Ihara, T., et al. (2008) *J. Biol. Chem. 283*, 23533−23541]. Here we cloned and expressed *Sr*SRI with its full-length transducer protein, *Sr*HtrI, as a fusion construct. We succeeded in producing the complex in *Escherichia coli* as a recombinant protein with high quality having all-*trans*-retinal as a chromophore for SRI, although the expression level was low (0.10 mg/L of culture). In addition, we report here the photochemical properties of the *Sr*SRI−*Sr*HtrI complex using time-resolved laser flash spectroscopy and other spectroscopic techniques and compare them to *Sr*SRI without *Sr*HtrI.

Microorganisms respond and adapt to photostimulation, in which light energy is absorbed by microbial rhodopsins, which are seven-transmembrane helix proteins containing retinal as a chromophore (*1*). Sensory rhodopsin I (SRI),[1] a photoactive membrane-embedded retinylidene protein, functions as a receptor regulating both negative and positive phototaxis in the archaeon *Halobacterium salinarum* (*2*, *3*). The original state of SRI and its long-lived photointermediate (the M-intermediate) are important for positive and negative phototaxis, respectively, and have absorption maxima at 587 and 373 nm, respectively (*2*). Sensory rhodopsin II (SRII, also known as phoborhodopsin) is a negative phototaxis receptor in haloarchaea, including *H. salinarum* and *Natronomonas pharaonis* (*3*, *4*). Those are called *Hs*SRII and *Np*SRII, respectively, and their absorption maxima are at ∼500 nm (*5*). Thus, haloarchaea are attracted to light with wavelengths longer than 520 nm, and they avoid light with wavelengths shorter than 520 nm due to the functions of SRI and SRII (*3*). Light with wavelengths of > 520 nm can activate the ion-pumping rhodopsins, bacteriorhodopsin (BR) and halorhodopsin (HR), to produce light energy, and cells avoid light of shorter wavelengths which contain harmful near-UV light.

The excitation light absorbed by *H. salinarum* SRI (*Hs*SRI) and *Np*SRII triggers *trans*−*cis* isomerization of the retinal chromophore that is covalently bound to a conserved lysine residue via a protonated Schiff base linkage (PSB) (*6*, *7*). This photoexcitation results in the sequential appearance of various photointermediates (K, L, M, and O) followed by a return to the unphotolyzed form of the protein (*3*, *8*). This linear cyclic photochemical reaction is called the photocycle. SRI and SRII form 2:2 signaling complexes with their cognate halobacterial transducer (Htr) proteins, HtrI and HtrII, respectively, are located in the cell membranes (*9*, *10*), and transmit light signals through changes in protein−protein interactions. Because the transducer proteins belong to a family of two-transmembrane helical methyl-accepting chemotaxis proteins (MCPs) (*11*), it is believed that SRI−HtrI and SRII−HtrII form ternary complexes with a kinase CheA and an adaptor protein CheW (*12*, *13*) and transmit signals to the flagellar motor, which controls the direction of rotation of the flagellar motor. For chemoreception in bacteria, MCP acts not only as a chemoreceptor but also as a transducer (*11*). On the other hand, for photoreception in archaea, the receptor (e.g., SRI and SRII) and the transducer (e.g., HtrI and HtrII) are separated, and direct interaction between them is required (*14*, *15*).

*Np*SRII is much more stable in the membrane and in detergent micelles than is *Hs*SRII (*16*), and an expression system of *Np*SRII and truncated *Np*HtrII having transmembrane segments

†This work was financially supported in part by Grants-in-Aid for Scientific Research (KAKENHI) on Priority Area (Area No. [477]) from the Ministry of Education, Culture, Sports, Science and Technology (MEXT) of Japan. This work was also supported by grants from the Japanese Ministry of Education, Culture, Sports, Science, and Technology to Y.F. (19042013 and 19045015), H.K. (19370067 and 20050015), and Y.S. (20050012).

*To whom correspondence should be addressed. Telephone: 81 52 789 2993. Fax: 81 52 789 3001. E-mail: z47867a@cc.nagoya-u.ac.jp.

[1]Abbreviations: DDM, *n*-dodecyl β-D-maltoside; HPLC, high-performance liquid chromatography; HtrI, halobacterial transducer protein for SRI; HtrII, halobacterial transducer protein for SRII; MCP, methyl-accepting chemotaxis protein; PSB, protonated Schiff base; BR, bacteriorhodopsin; HR, halorhodopsin; SRI, sensory rhodopsin I; SRI−HtrI, complex of SRI and HtrI; SRII, sensory rhodopsin II; *Sr*SRI−*Sr*HtrI(1−128), fusion complex of *Sr*SRI and truncated *Sr*HtrI expressed from position 1 to 128.

required for their interaction can be used to produce large amounts of those proteins (*17*, *18*). Therefore, *Np*SRII and *Np*HtrII have been well-characterized over the past few years (*19*). In the case of SRI−HtrI, Minorova et al. reported an interesting result by using a fusion protein with *Hs*SRI and a shortened *Hs*HtrI (*20*). Recently, Engelhard and co-workers succeeded in expressing full-length *H. salinarum* HtrII as a recombinant protein (*21*). In 2005, Mongodin et al. reported the genomic sequence of the eubacterium *Salinibacter ruber* and discovered two genes encoding sensory rhodopsin I-like proteins (*22*). Recently, we cloned and expressed them as recombinant proteins, and one was expressed well in the bacterial membrane with retinal and was named *Salinibacter* sensory rhodopsin I (*Sr*SRI) (*23*). In addition to the expression system, the high stability of *Sr*SRI makes it possible to prepare large amounts of the protein and enables studies of mutant proteins. Thus, *Sr*SRI is expected to allow new approaches to the investigation of the photosignaling process of SRI−HtrI.

Here we characterized *Sr*SRI with its transducer protein, *Sr*HtrI, as a full-length fusion construct. The complex was expressed in *Escherichia coli* membranes as a recombinant protein having all-*trans*-retinal as a chromophore of SRI. We also report here the effects of *Sr*HtrI binding to *Sr*SRI on photochemical reactions of the *Sr*SRI−*Sr*HtrI complex using time-resolved laser flash spectroscopy and other spectroscopic techniques and compare them to those of *Sr*SRI without *Sr*HtrI. In addtion, the truncated *Sr*HtrI was used here to analyze the effects of the reconstitution into the PG liposomes.

MATERIALS AND METHODS

Plasmids and Strains. *S. ruber* (a kind gift from Dr. Dyall-Smith, The Max Planck Institute of Biochemistry, Martinsried, Germany) was grown aerobically at 40 °C and pH 7.0 in medium: 195 g/L NaCl, 25 g/L $MgSO_4 \cdot 7H_2O$, 16.3 g/L $MgCl_2 \cdot 6H_2O$, 1.25 g/L $CaCl_2 \cdot 2H_2O$, 5.0 g/L KCl, 0.25 g/L $NaHCO_3$, 0.625 g/L NaBr, and 1.0 g/L yeast extract (Difco, Detroit, MI). Cells were harvested by centrifugation and were stored at −80 °C. Genomic DNA was prepared using the method of Marmur (*24*). *E. coli* DH5α was used as a host for DNA manipulation, and BL21-(DE3) was used for expressing the genes. For DNA manipulation, the transducer gene for sensory rhodopsin I (SRU_2510) was amplified using PCR from the genomic DNA of *S. ruber*. The forward primer (5′-CGTCGGCGTCGAACGGCGCGTCG-GCGATGAAACGCTTTCTG-3′) and the reverse primer (5′-CCGCTCGAGTGCCCCGAGCTCCGGCGCC-3′) for the *Sr*SRI−*Sr*HtrI fusion gene were designed (underlining indicates the restriction site for *Xho*I). The stop codon was deleted during amplification, generating a linker region between *Sr*SRI and *Sr*HtrI that contains 11 residues (Thr-Ser-Ala-Ser-Ala-Ser-Asn-Gly-Ala-Ser-Ala). The *Sr*SRI−-*Sr*HtrI fusion gene was constructed by PCR with the two-step mutagenesis method using the pTK001 plasmid as a template. The *Nde*I and *Xho*I fragment was ligated to the *Nde*I and *Xho*I sites of the pET21c(+) vector (Novagen, Madison, WI). Consequently, the plasmid encodes six histidines at the C-terminus, and it was named pSrST3. This cloning strategy resulted in the following N- and C-terminal peptide sequences: $^{1(SrSRI)}$MDPI...ELGA$^{518(SrHtrI)}$LEHHHH-HH. The constructed plasmid was analyzed using an automated sequencer to confirm the expected nucleotide sequence. The *Sr*SRI−*Sr*HtrI(1−128) fusion gene was constructed in the same way.

Protein Expression and Purification. Cells were grown in LB medium supplemented with ampicillin (final concentration of 50 μg/mL). *E. coli* BL21(DE3) harboring pSrST3 was grown to an OD_{660} of 0.3−0.5 in a 30 °C incubator, followed by the addition of 0.5 mM IPTG and 10 μM all-*trans*-retinal. Cells were harvested 5 h postinduction by centrifugation at 4 °C, resuspended in buffer [50 mM MES (pH 6.5)] containing 1 M NaCl, and then disrupted by sonication. Cell debris was removed by low-speed centrifugation (5000*g* for 10 min at 4 °C). Preparation of crude membranes and purification of protein were conducted as described previously (*18*, *23*). For solubilization of the membranes, 1% (w/v) *n*-dodecyl β-D-maltoside (DDM) was added and the suspension was incubated overnight at 4 °C. The solubilized membrane extracts were isolated by high-speed centrifugation (100000*g* for 30 min at 4 °C), and the supernatants were applied to a Ni affinity column (HisTrap, GE Healthcare, Uppsala, Sweden) at 4 °C in the dark. Thereafter, the column was washed extensively with buffer [50 mM MES (pH 6.5)] containing 1 M NaCl, 20 mM imidazole, and 0.1% (w/v) DDM to remove unspecifically bound proteins. The histidine-tagged proteins were then eluted with buffer [0.1% DDM, 1 M NaCl, 50 mM Tris-HCl (pH 7.0), and 300 mM imidazole]. The eluted protein was then further purified with a gel-filtration column (Superdex 200HR, Amersham Biosciences, Pittsburgh, PA) in buffer containing 0.1% DDM, 1 M NaCl, and 50 mM Tris-HCl (pH 7.0). Unexpectedly, full-length *Sr*SRI−*Sr*HtrI was not reconstituted into PG or PC liposomes via removal of the detergent with Bio-Beads (SM-2, Bio-Rad, Hercules, CA), and therefore, we used *Sr*SRI−*Sr*HtrI in the detergent as the sample. *Sr*SRI without *Sr*HtrI was purified as described previously (*23*). Briefly, the sample was solubilized by DDM and purified with a Ni affinity column and an anion exchange column. The purified *Sr*SRI with or without *Sr*HtrI was dissolved in sodium dodecyl sulfate−polyacrylamide gel electrophoresis (SDS−PAGE) loading buffer containing 5% 2-mercaptoethanol and was subjected to 10% acrylamide SDS−PAGE. Immunoblotting was performed using an anti-His tag antibody (GE Healthcare). *Sr*SRI−*Sr*HtrI(1−128) posseissing a histidine tag at the C-terminus was expressed in *E. coli* [BL21(DE3)], solubilized with 1.0% DDM, and purified with a Ni column. The purified protein was reconstituted into L-α-phosphatidylglycerol (PG) liposomes (*Sr*SRI−*Sr*HtrI:PG molar ratio of 1:50), where DDM was removed with Bio-Beads (SM-2, Bio-Rad).

UV−Vis Spectroscopy and HPLC Analysis. The sample was concentrated and exchanged with an Amicon Ultra instrument (Millipore, Bedford, MA) against media with compositions as described later. UV−vis spectra were recorded using a UV2450 spectrophotometer with an ISR2200 integrating sphere (Shimazu, Kyoto, Japan). For the pH titration experiments, the DDM-solubilized sample was washed and resuspended in six buffers (citric acid, MES, HEPES, MOPS, CHES, and CAPS, each at a concentration of 10 mM) with 1 M NaCl and 0.1% DDM. The buffer composition had the same buffer capacity over a wide range of pH values (2−9). pH values of the sample suspensions were measured using a SevenEasy pH-meter with a 9811 glass electrode (Metller Toledo, Tokyo, Japan). High-performance liquid chromatography (HPLC) analysis was performed as described previously (*23*). Briefly, the purified sample was analyzed in buffer [0.1% DDM, 1 M NaCl, and 50 mM Tris-HCl (pH 7.0)]. The HPLC system consisted of a PU-2080 pump and an UV-2075 UV−vis detector (Jasco, Tokyo, Japan). The chromatograph was equipped with a silica column (6.0 mm × 150 mm,

YMC-Pack SIL); the solvent was 12% (v/v) ethyl acetate and 0.12% (v/v) ethanol in hexane, and the flow rate was 1.0 mL/min. Extraction of retinal oxime from the sample was accomplished with hexane after denaturation in methanol and 500 mM hydroxylamine at 4 °C. The molar composition of retinal isomers was calculated from the areas of the peaks monitored at 360 nm. Assignment of each peak was performed by comparing it with the HPLC pattern from retinal oximes of authentic all-*trans*- and 13-*cis*-retinals. Two independent measurements were averaged.

Time-Resolved Laser Spectroscopy. For the flash photolysis experiment on the microsecond time scale (decay of the K intermediate), we used second-harmonic light from a Nd^{3+}:YAG laser (λ = 532 nm, pulse width ~ 6 ns, Minilite II Continuum, Santa Clara, CA) as a pump pulse. The energy of the pump pulse was 50 μJ/pulse. The pump beam was focused onto the sample solution with a lens. A Xe lamp (Hamamatsu Photonics, Hamamastu, Japan) was used as a probe source which enabled us to measure the absorption change of the sample solution after excitation over a range from 490 to 740 nm, and it was focused onto the sample from the opposite side of the pump beam. After being transmitted through the solution, the probe light was collected with a lens and was led into an optical fiber which was attached to a polychrometer (SpectraPro 2300i, Princeton Instruments/Acton, Trenton, NJ). The dispersed probe light was projected onto an ICCD camera system (PI-MAX/PI-MAX2 System, Princeton Instruments) so the transmitted light intensity could be monitored at various wavelengths. We measured the transient absorption spectra at various time points after the excitation by changing the timing delay between the pump pulse and the ICCD gate. For measurement of the time trace of the absorption change at a specific wavelength, the probe light was reflected by a flipper mirror to another monochromator, and the absorption change was monitored with a photomultiplier (1P28, Hamamatsu Photonics) and a digital oscilloscope (TDS-3052, Tektronix, Beaverton, OR). Sample solutions were placed in quartz cells, and the absorbance was adjusted to ~0.5 at the excitation wavelength. The sample was excited with a pump beam every ~5 min. The temperature of each sample was kept at 25 °C during the measurement.

For measurements of the M intermediate, the apparatus and the procedure for analysis were essentially as described previously (*25*). Each purified sample was resuspended in buffer [50 mM Tris-HCl (pH 7.0) and 0.1% DDM] with 1 M NaCl. Flash-induced absorption changes were acquired with a 20 ms interval using a commercial flash photolysis system (Hamamatsu Photonics K.K., Hamakita, Japan). Excitation of each *Sr*SRI sample was accomplished using 545 nm nanosecond laser pulses from a Nd:YAG laser apparatus (LS-2134UT-10; LOTIS TII, 355 nm, 7 ns, 60 mJ) through an optical parametric oscillator (OPO) (LT-2214-OPO/PM; LOTIS TII). The energy of one laser pulse was 3.3 mJ. Subsequent spectral changes upon laser excitation were collected consecutively. Therefore, one series of difference spectra was measured for one excitation. The sample was excited with a pump beam every ~5 min. For signal-to-noise improvement, 40 photoreactions were averaged for each sample solution. The absorbance at λ_{max} (547 nm) was 0.60 and 0.48 before and after the experiment, respectively (the laser-induced bleach of the sample was 20%), while the kinetics of the two experiments were almost identical. The temperature of each sample was kept at 25 °C. For the time-resolved strobe flash spectroscopy, the apparatus and the procedure for analysis were essentially as described previously (*25*).

RESULTS AND DISCUSSION

SrHtrI and Its Related Proteins. The gene for *Sr*SRI (SRU_2511) has a downstream sequence immediately followed by the second gene in a probable operon under the control of the same promoter as *Sr*SRI. The putative transducer gene (SRU_2510, Htr for SRU_2511) encodes a 518-residue protein with two transmembrane domains at the N-terminal portion followed by an extensive domain with primarily hydrophilic residues. SRU_2510 is hereafter called *Sr*HtrI. This topology is similar to that of the Htr transducers from the archaeon *H. salinarum*. The eubacterium *S. ruber* also has two light-driven ion pumps, xanthorhodopsin and a halorhodopsin-like protein, making an energy source for living cells (*22*, *26*). The *Sr*SRI−*Sr*HtrI complex is expected to function as a positive phototaxis sensor against longer wavelengths of light where ion-pumping rhodopsins can utilize light energy and as a negative phototaxis sensor against shorter wavelengths of light that contain harmful UV rays. Glu56, one of the most important residues for phototaxis signaling in *Hs*HtrI (*27*), is replaced with Ile in *Sr*HtrI (SRU_2510), whereas Tar and Tsr (MCPs of *E. coli*) have Leu at this site, which is similar to situation in *Sr*HtrI (*11*).

Protein Expression, Purification, and Absorption Spectrum. Using PCR, we obtained a fragment containing the full length of the SRU_2510 gene coding region and its truncated fragments (*Sr*HtrI[1−128] and *Sr*HtrI[1−194]). An *Nde*I site was created at the translation initiation site in the PCR product using an oligonucleotide primer containing the *Nde*I site. An *Xho*I site was created, and the stop codon was deleted during the amplification. The *Nde*I and *Xho*I fragment of the PCR product was then cloned into the *Nde*I and *Xho*I sites of pET21c(+). Full-length *Sr*HtrI was expressed well in *E. coli*; however, the proteins were digested and/or degraded during the solubilization and purification as judged by SDS−PAGE and Western blotting detected by the C-terminal histidine tag even in the presence of a protease inhibitor cocktail (Complete, EDTA-free, Roche, Mannheim, Germany) (data not shown). This is consistent with the previous report that *Hs*HtrI is not stable without *Hs*SRI (*28*). Therefore, in this study, we linked *Sr*HtrI to *Sr*SRI with a flexible linker region (Figure 1). The peptide sequence of that linker contains 11 residues (Thr-Ser-Ala-Ser-Ala-Ser-Asn-Gly-Ala-Ser-Ala), which comprise an unstructured region, and was previously used for the linkage between *Np*SRII and *Np*HtrII (*15*), *Hs*SRII and *Hs*HtrII (*29*), and the mutant of *H. salinarum* bacteriorhodopsin [*Hs*BR(T)] and *Hs*HtrII (*30*). These fusion proteins exhibited phototaxis responses with the same efficiency as the wild-type SRII−HtrII complex, implying that this linker region does not influence normal structural changes in both sensory rhodopsin and HtrII, or the signaling. Also, in the case of *Hs*SRI−*Hs*HtrI, the fusion protein shows phototaxis responses and proper structural changes as reported previously (*9*).

Figure 2a shows SDS−PAGE patterns of purified *Sr*SRI alone and in the *Sr*SRI−*Sr*HtrI complex by Coomassie Brilliant Blue staining (CBB, left panel) and by Western blot analysis of the proteins using an anti-His tag antibody (WB, right panel). The apparent molecular masses of the main bands are 26.7 and 82.8 kDa which correspond well to the expected values for *Sr*SRI alone and *Sr*SRI-*Sr*HtrI, respectively. Figure 2a also shows that *Sr*SRI alone and *Sr*SRI−*Sr*HtrI are purified in adequate quantities (~3.0 mg/L of culture for *Sr*SRI and 0.10 mg/L of culture for *Sr*SRI−*Sr*HtrI) with high quality and shows that *Sr*SRI and *Sr*SRI−*Sr*HtrI form estimated dimer/trimers and

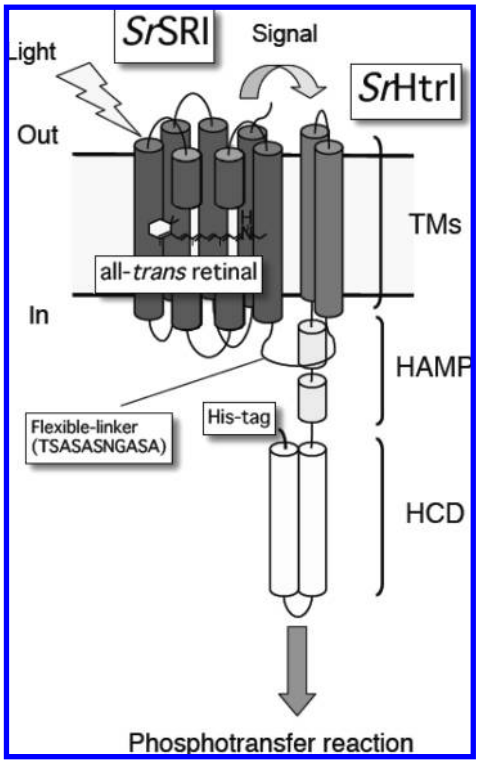

FIGURE 1: Schematics of *Sr*SRI and its cognate transducer protein, *Sr*HtrI. The C-terminus of *Sr*SRI is connected to *Sr*Htrl by a short flexible linker that contains 11 residues (Thr-Ser-Ala-Ser-Ala-Ser-Asn-Gly-Ala-Ser-Ala). For purification and detection, a His tag was added to the C-terminus of *Sr*HtrI. *Sr*SRI−*Sr*HtrI forms a ternary complex with kinase CheA and adaptor protein CheW and activates the phosphorylation cascades that modulate the flagellar motor. TMs and HCD denote transmembrane segments and the highly conserved domain, respectively. HAMP is a cytoplasmic domain which is typically found in various proteins such as histidine kinases, adenylylcyclases, MCPs, and phosphatases (*46*). The HAMP domain plays crucial roles in the phosphorylation or methylation of homodimeric receptors by transmitting conformational changes from the periplasmic to the cytoplasmic domain (*47*).

dimers, respectively (asterisks in Figure 2a), because these bands are detected in both CBB and WB. It has been reported that the dimer of *Hs*HtrI is sandwiched between two molecules of *Hs*SRI (*9*) and that MCPs including HtrI and HtrII form homodimers in the membrane (*11*). Thus, we speculate that the SDS-resistant homodimer of *Sr*SRI−*Sr*HtrI detected here may be a functionally important form.

The absorption spectra of purified *Sr*SRI alone and *Sr*SRI−*Sr*HtrI were obtained as shown in Figure 2b. The sample was concentrated and exchanged with Amicon Ultra apparatus (Millipore) against a buffer [50 mM Tris-HCl (pH 7.0)] containing 0.1% DDM and 1 M NaCl. The absorption maximum of *Sr*SRI−*Sr*HtrI is at 544 nm, which is shifted from 557 nm in a *Sr*HtrI-dependent manner, implying that *Sr*HtrI interacts with *Sr*SRI and perturbs the retinal chromophore of *Sr*SRI. We previously reported that the absorption maximum of *Sr*SRI alone is shifted from 544 to 557 nm in a Cl^--dependent manner (*25*), while the Cl^--induced spectral red shift (532 → 544 nm) was also observed in *Sr*SRI−*Sr*HtrI (data not shown). Thus, the absorption maxima of *Sr*SRI(Cl^--free), *Sr*SRI(Cl^-), *Sr*SRI−*Sr*HtrI(Cl^--free), and *Sr*SRI−*Sr*HtrI(Cl^--free) were observed at 544, 557, 532, and 544 nm, respectively, indicating that the spectral blue shift for *Sr*HtrI binding (from 557 to 544 nm) is not caused by the effect of Cl^-.

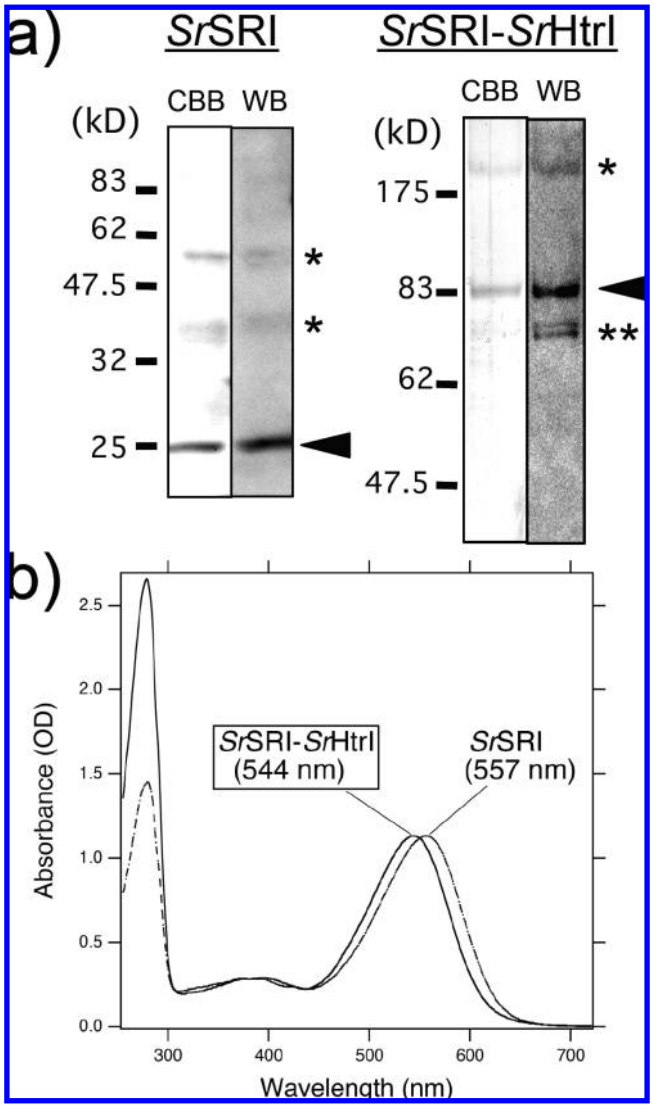

FIGURE 2: (a) SDS−PAGE patterns of purified *Sr*SRI alone and *Sr*SRI−*Sr*HtrI, and their immunoblotting by an anti-His tag antibody. Asterisks denote estimated oligomers. (b) Absorption spectra of *Sr*SRI alone and *Sr*SRI−*Sr*HtrI, which have absorption maxima of 557 and 544 nm, respectively. The purified *Sr*SRI with or without *Sr*HtrI was resuspended in a buffer [50 mM Tris-HCl (pH 7.0)] containing 0.1% DDM and 1 M NaCl.

Retinal Configuration and pK_a Value of the Counterion. To investigate whether the spectral change was caused by the difference in retinal configuration, we used HPLC analysis, since it is well-known that a decrease in the level of the 13-*cis*-retinal isomer causes a spectral red shift in microbial rhodopsins (*31*). Figure 3 shows the retinal isomer composition. The *Sr*SRI−*Sr*HtrI complex in the dark contains more than 95% all-*trans*-retinal with a small proportion of 13-*cis*-retinal as well as the *Sr*SRI−*Sr*HtrI complex with light accumulation as well as *Sr*SRI without *Sr*HtrI, indicating that the spectral red shift is not caused by a change in retinal configuration. In retinal proteins (except for HR), the protonated retinal Schiff base is stabilized by a deprotonated aspartate as a counterion (Asp72 for *Sr*SRI) (Figure 4a). It was reported that the pK_a value of the Asp76 residue of *Hs*SRI is elevated from 7.2 to 8.5 upon association with *Hs*HtrI (*32*). Using the *Sr*SRI−*Sr*HtrI complex, a spectroscopic pH titration was performed to estimate the pK_a value of Asp72. Difference spectra from pH 8.6 to 6.5, 5.8, 5.1, and 4.7 were shown over a spectral range from 465 to 720 nm (Figure 4b). The

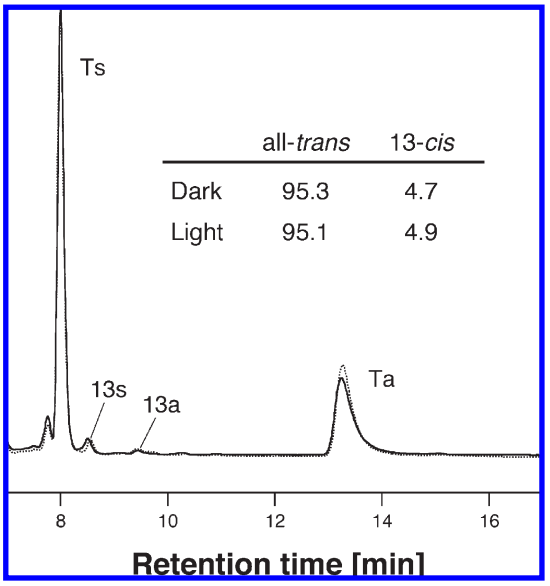

FIGURE 3: Chromophore configuration extracted from *Sr*SRI−*Sr*HtrI in the dark (—) and in the light (···). The detection beam was set at 360 nm. Ts, Ta, 13s, and 13a stand for all-*trans*-15-*syn*-retinal oxime, all-*trans*-15-*anti*-retinal oxime, 13-*cis*-15-*syn*-retinal oxime, and 13-*cis*-15-*anti*-retinal oxime, respectively. The molar composition of retinal isomers was calculated from the areas of the peaks in the HPLC patterns. The light-adapted form was produced by illumination of *Sr*SRI−*Sr*HtrI with > 520 nm light for 1 min at 4 °C. That light intensity is sufficient to convert *Anabaena* sensory rhodopsin (ASR) and bacteriorhodopsin (BR) into the light-adapted forms.

spectra were recorded in the pH range from 8.57 to 4.68 because a denatured form occurred in a buffer containing 1 M NaCl and 0.1% DDM. The sample was unstable under the acidic conditions (pH < 4.6). The results were fit well to the Henderson−Hasselbach equation (*33*) with a single pK_a (Figure 4c), and the pK_a value of Asp72 for *Sr*SRI−*Sr*HtrI was estimated to be 4.9 compared with the previously reported pK_a value of 4.3 for *Sr*SRI alone (dotted lines in Figure 4c) (*23*). Thus, these results indicate that the pK_a value of Asp72 is elevated from 4.3 to 4.9 upon *Sr*HtrI association, although the shift value of the *Sr*SRI−*Sr*HtrI complex (0.6 unit) is smaller than that of *Hs*SRI−*Hs*HtrI (1.3 units). In the case of SRII, no shift was observed. The lower pK_a of *Sr*SRI−*Sr*HtrI (4.9) versus that of *Hs*SRI−*Hs*HtrI (8.5) also indicates that counterion Asp72 exists in a deprotonated form at neutral pH where the bacteria live, suggesting the functional importance of the deprotonated state of the *Sr*SRI−*Sr*HtrI complex.

Effects of SrHtrI Binding to SrSRI on Its Photocycle. *Sr*SRI absorbs orange light and triggers a cyclic reaction that is comprised of a series of intermediates, designated alphabetically (K and M intermediates) (*23*). An important question is whether the photocycle of *Sr*SRI is affected by *Sr*HtrI binding. The *trans*−*cis* photoisomerization of the retinal chromophore leads to the formation of the red-shifted K intermediate. We analyzed the effects of binding of *Sr*HtrI to *Sr*SRI on the decay rate constant of the K intermediate and its molar extinction coefficient. The light minus dark difference absorption spectra were obtained over a time range from 300 ns to 100 μs (Figure 5a). We assigned the positive band at 640 nm and the negative band at 555 nm to the red-shifted K intermediate accumulation and ground state bleaching, respectively. The spectral red shift indicates the formation of the K intermediate of the *Sr*SRI−*Sr*HtrI complex,

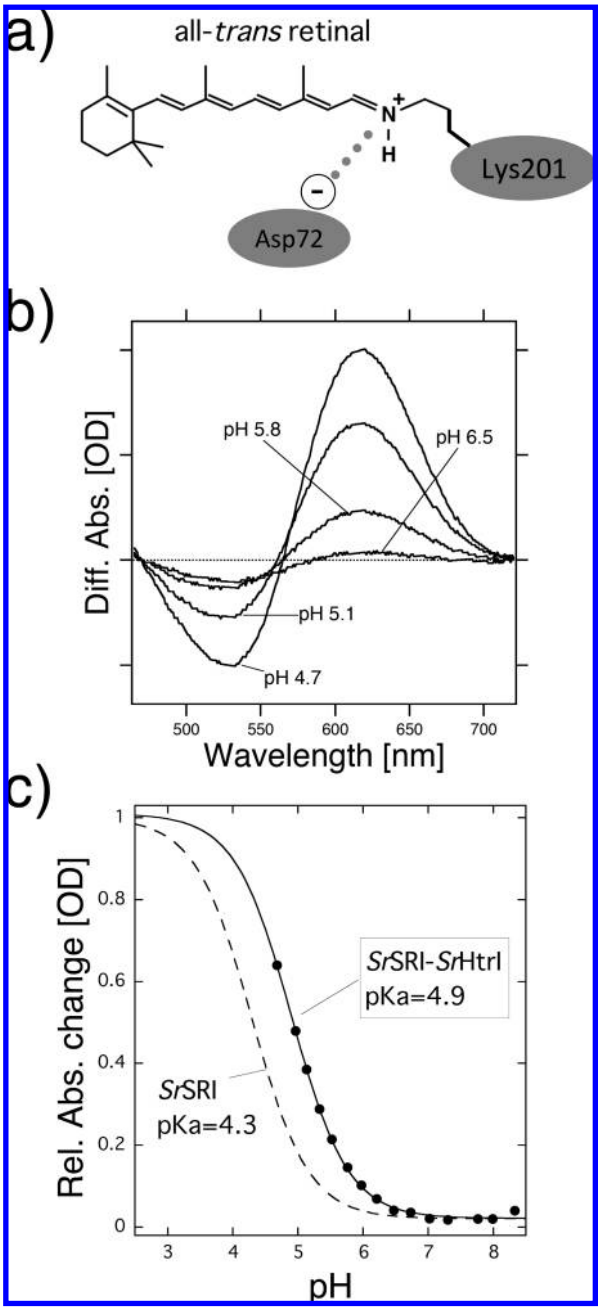

FIGURE 4: (a) Chemical structure of the chromophore of *Sr*SRI. The retinal chromophore is covalently bound to a conserved lysine residue (Lys201) via a PSB linkage, which is stabilized by its counterion, Asp72. (b) pH titration curves of the counterion, Asp72, in *Sr*SRI−*Sr*HtrI. The sample was suspended in a mixture of six buffers with 1 M NaCl. (c) The titration curves were analyzed using the Henderson−Hasselbalch equation with a single pK_a value. The temperature was kept at 20 °C. Data for *Sr*SRI alone with 1 M NaCl were reproduced from a previous study (*22*) for the sake of comparison. One division of the *y*-axis of panel b corresponds to 40 mOD units.

while the molar extinction coefficient decreased in the complex as compared with that of *Sr*SRI alone with Cl^- (*23*). The lowered extinctions for an intermediate of *Hs*SRI, the K intermediate of *Np*SRII, and the K intermediate of *Sr*SRI alone without Cl^- are also reported by Swartz et al. (*34*), Chizhov et al. (*35*), and Suzuki et al. (*25*), respectively. Figure 5b shows the time course of the absorbance changes at 640 nm in solutions containing 1 M NaCl and 0.1% DDM. Recently, we reported that 1 M NaCl is sufficient for *Sr*SRI to bind the chloride ion because the

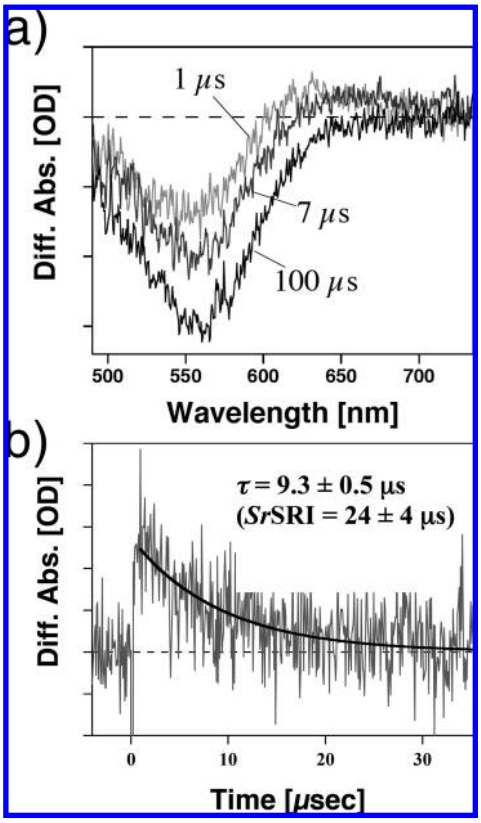

FIGURE 5: Flash-induced difference absorption spectra of *Sr*SRI−*Sr*HtrI with 1 M NaCl and 0.1% DDM over a spectral range from 490 to 730 nm and a time range from 300 ns to 100 μs. Curves in panel a are spectra 1, 7, and 10 μs after the illumination. (b) Flash-induced kinetic data of *Sr*SRI−*Sr*HtrI at 640 nm representing the K decay. The data fit well with a single-exponential decay equation, and the lifetime was estimated to be 9.3 ± 0.5 μs for *Sr*SRI−*Sr*HtrI and 24 ± 4 μs for *Sr*SRI without *Sr*HtrI. The temperature was kept at 25 °C. One division of the *y*-axis of panels a and b corresponds to 0.05 and 0.005 absorbance unit, respectively.

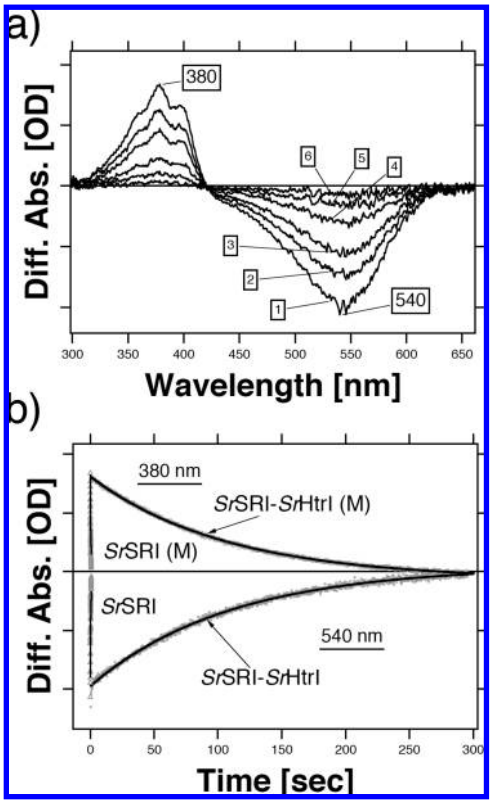

FIGURE 6: (a) Flash-induced difference spectra of *Sr*SRI−*Sr*HtrI over the spectral range from 300 to 660 nm on a millisecond to second time scale. Curves 1−6 are spectra 0.2 (1), 30 (2), 60 (3), 120 (4), 180 (5), and 240 s (6) after the illumination. The temperature was kept at 25 °C. (b) Flash-induced kinetic data of *Sr*SRI−*Sr*HtrI at 380 nm representing the M decay and at 540 nm representing the recovery of the original *Sr*SRI−*Sr*HtrI. The kinetic data of *Sr*SRI alone were reproduced from ref *23* for comparison of the time range with that of the *Sr*SRI−*Sr*HtrI complex. For *Sr*SRI alone, the M intermediate and the unphotolyzed state were monitored at 390 and 556 nm, respectively. The data fit well with a single-exponential decay equation. One division of the *y*-axis of panels a and b corresponds to 0.1 OD unit.

K_m value was ~300 mM (*25*). In fact, the curves fit well to a single-exponential decay equation, and the lifetimes were estimated to be 9.3 ± 0.5 μs for *Sr*SRI−*Sr*HtrI and 24 ± 4 μs for *Sr*SRI without *Sr*HtrI (*25*), indicating that the decay rate of the K intermediate of *Sr*SRI−*Sr*HtrI is 2.6-fold faster than that of *Sr*SRI alone, indicating the influence of *Sr*HtrI association with the retinal chromophore of *Sr*SRI.

Figure 6a shows the flash-induced difference spectrum of the *Sr*SRI−*Sr*HtrI complex over the spectral range from 300 to 660 nm on a millisecond to second time scale. At 380 nm, an increase and a decrease in absorbance were observed, implying the formation and decay of an intermediate $SrSRI_M$−*Sr*HtrI similar to $HsSRI_M$−*Hs*HtrI(S373) where an absorbance maximum is located at 373 nm (*2*). Figure 6b shows the time courses of the absorbance change at selected wavelengths (380 nm for the M state and 540 nm for the unphotolyzed state). The M decay rate is estimated to be 0.0094 s^{-1} by a single-exponential equation, indicating that the M decay of *Sr*SRI−*Sr*HtrI is 640-fold slower than that of *Sr*SRI alone (Figure 6b). This slow photocycle is particularly important because a key difference between transport and sensory rhodopsins is the much slower kinetics of the photochemical reaction cycle of the sensors (*30*). The ion-pumping rhodopsins (BR, HR, and proteorhodopsin) have been optimized by nature for fast photocycling rates to make them efficient pumps (*36*, *37*). In contrast, the sensory rhodopsins *Hs*SRI and *Np*SRII have slow photocycles, which allows the transient accumulation of long-lived signaling states of the receptors to catalyze a sustained phosphorylation cascade, including CheA and CheY that controls flagellar motor rotation (*3*, *38*). The slow photocycle of *Sr*SRI associated with *Sr*HtrI therefore is a property similar to that of sensory rhodopsins. Spudich and co-workers reported that the M decay of *Hs*SRI is affected by environmental pH, whereas the *Hs*SRI−*Hs*HtrI complex is not (*9*, *39*). Figure 7 shows the light-induced absorbance changes of the M intermediate and the unphotolyzed state in *Sr*SRI alone (a) and the *Sr*SRI−*Sr*HtrI complex at pH 6 and 8. The gray lines show the fitting curves with a single-exponential equation. Unlike that of *Hs*SRI, the M decay of *Sr*SRI−*Sr*HtrI is accelerated at pH 6.0, whereas *Sr*SRI alone is not affected. It is well-known that the M intermediate of *Hs*SRI(S373) is activated by UV and forms a two-photon product P510, which is important for negative phototaxis (*2*, *40*). *Sr*SRI without *Sr*HtrI also forms a P510-like intermediate by two-photon excitation (*23*). Though we tried to accumulate the two-photon product using two laser flashes, *Sr*SRI−*Sr*HtrI forms almost undetectable levels of a P510-like photointermediate (data not shown), suggesting that its rate of decay is rapid relative to its rate of formation under these conditions.

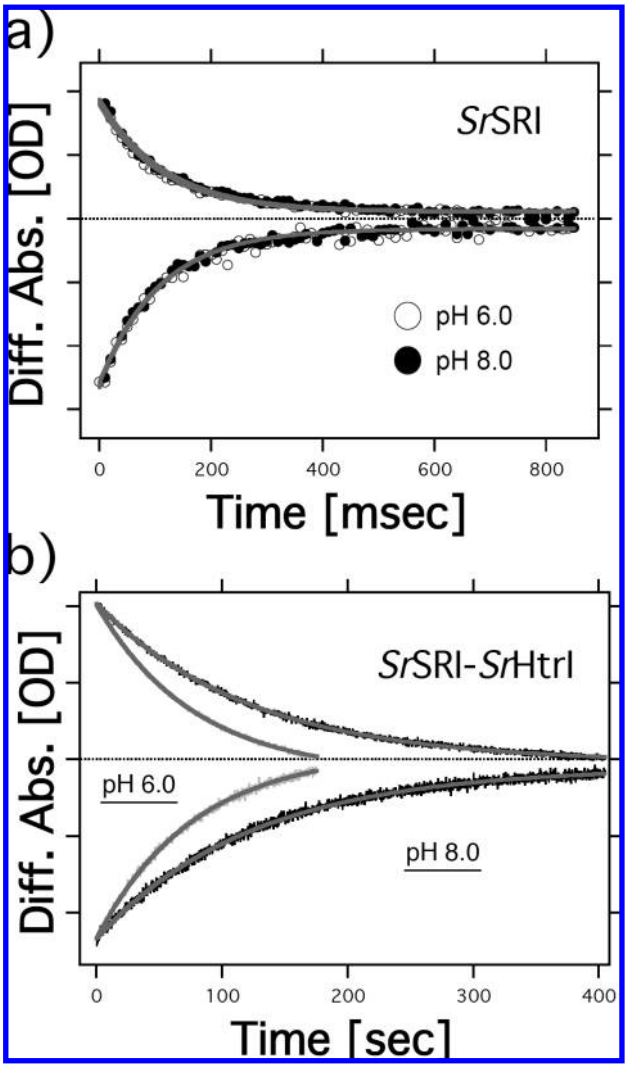

FIGURE 7: (a) Flash-induced kinetic data of *Sr*SRI−*Sr*HtrI at pH 6.0 (○) and pH 8.0 (●) in a buffer containing 1 M NaCl, 50 mM Tris-HCl, and 0.1% DDM. The M decay rates are estimated to be 6 s^{-1} for pH 6.0 and pH 8.0 by a single-exponential equation (gray lines), and the values are identical to that of *Sr*SRI−*Sr*HtrI at pH 7.0. The data fit well with a single-exponential decay equation. (b) Flash-induced kinetic data of *Sr*SRI−*Sr*HtrI at pH 6.0 (gray) and pH 8.0 (black) in a buffer containing 1 M NaCl, 50 mM Tris-HCl, and 0.1% DDM. The M decay rates are estimated to be 0.013 s^{-1} for pH 6.0 and 0.0083 s^{-1} for pH 8.0 by a single-exponential equation (gray lines), and the values are significantly different from that of *Sr*SRI−*Sr*HtrI at pH 7.0 (0.0094 s^{-1}). The data fit well with a single-exponential decay equation. One division of the *y*-axis of panels b and c corresponds to 30 and 40 mOD units, respectively.

Sensory Rhodopsins with Their Cognate Transducer Proteins. The similarities and differences between sensory rhodopsins with their cognate transducer proteins demonstrated in this study are summarized in Table 1. Here it should be noted that M decay of *Hs*SRI−*Hs*HtrI is pH-independent between pH 5 and 8 but becomes pH-dependent above this pH range, where the receptor's Asp76 is deprotonated. The Htr-induced 13 nm spectral blue shift is a unique feature of *Sr*SRI (Figure 2b), while the upper shift in pK_a of a counterion Asp residue by the cognate transducer protein is common among *Sr*SRI and *Hs*SRI in contrast to SRII (Figure 4), which suggests that this feature is important for SRIs. The pH dependence of the M decay was observed in *Sr*SRI and SRII (*41*), but not in *Hs*SRI (Figure 7) (*39*). However, *Sr*SRI, *Hs*SRI, and SRII with or without HtrI or HtrII have slow photocycling rates compared with the ion-pumping rhodopsins, BR and HR (*38*). By using FTIR spectroscopy, several groups have reported that structural changes in Asn74 of *Np*HtrII and Asn53 of *Hs*HtrI were caused by light activation of the cognate sensory rhodopsin (*20*, *42*, *43*). Residues Asn74 and Asn53 were replaced with Arg and Thr in *Sr*HtrI, respectively. This may be related to the differences in photocycle and structural changes among sensory rhodopsin−transducer complexes. The molecular origin of these differences needs to be investigated in the future. In this study, the roles of *Sr*HtrI and *Sr*SRI are suggested to be the stabilization of *Sr*HtrI by *Sr*SRI as well as *Hs*SRI and *Hs*HtrI, and a decrease in the decay rate constant of the active M intermediate of *Sr*SRI by *Sr*HtrI. Sensory rhodopsins (SRI and SRII) are suggested to form complexes not only with HtrIs but also with CheW and CheA through HtrI (*38*). The effect(s) of binding of CheW, CheA, and CheY on *Sr*SRI and *Sr*HtrI will be our next focus of study.

Table 1: Effects of the Cognate Transducer Protein Htrl Binding to Sensory Rhodopsin I and II

	retinal	pK_a	λ_{max} (nm)	pH dependence (M decay)
*Sr*SRI	all-*trans*	+0.6	−13	yes
*Hs*SRI	all-*trans* (*40*)	+1.3 (*32*)	0 (*38*)	no (*39*)
*Np*SRII	all-*trans* (*44*)	0 (*4*)	0 (*45*)	yes (*41*)

Effect of Reconstitution into the PG Liposomes. We analyzed here whether the reconstitution of *Sr*SRI−*Sr*HtrI into the lipids affects the photochemical properties. As described, full-length *Sr*SRI−*Sr*HtrI was not reconstituted into PG or PC liposomes, and therefore, we used here the fusion complex of *Sr*SRI and truncated *Sr*HtrI(1−128). *Sr*HtrI(1−128) has two transmembrane segments (Figure 1) and a domain structure similar to that of *Np*HtrII(1−159) (*18*). Figure 8a shows the absorption spectrum of *Sr*SRI−*Sr*HtrI(1−128) in the DDM micelles. The sample was concentrated and exchanged with an Amicon Ultra apparatus (Millipore) against a buffer [50 mM Tris-HCl (pH 7.0)] containing 0.1% DDM and 1 M NaCl. The absorption maximum of *Sr*SRI−*Sr*HtrI(1−128) is 544 nm, which is the almost identical to that of full-length *Sr*SRI−*Sr*HtrI-(1−128), implying that *Sr*HtrI(1−128) interacts with *Sr*SRI as well as full-length *Sr*HtrI, while the absorption maximum of reconstituted *Sr*SRI−*Sr*HtrI(1−128) in PG liposomes is 550 nm, indicating that PG lipids perturb the retinal chromophore of *Sr*SRI. Figure 8 also shows the strobe flash-induced difference spectrum of the *Sr*SRI−*Sr*HtrI complex in the DDM micelles (b) and the PG liposomes (c). The M decay rates are estimated by a single-exponential equation to be 0.0121 s^{-1} for the solubilized sample and 0.0114 s^{-1} for the reconstituted sample, and these values are similar to that of full-length *Sr*SRI−*Sr*HtrI (0.0094 s^{-1}) (Figure 6b). The recovery rates were also estimated by a single-exponential equation to be 0.0115 s^{-1} for the solubilized sample and 0.0103 s^{-1} for the reconstituted sample. These results indicate that both truncation and reconstitution into the PG lipids have almost no effect on the M decay and recovery of *Sr*SRI−*Sr*HtrI. Thus, the photocycle rates in both detergent micelles and proteoliposomes are very slow with half-times of >50 s. Phototaxis by swimming prokaryotic cells operates on the time scale for light gradient sensing of ∼0.5−3 s, depending on swimming speed. Therefore, the slow cycles are

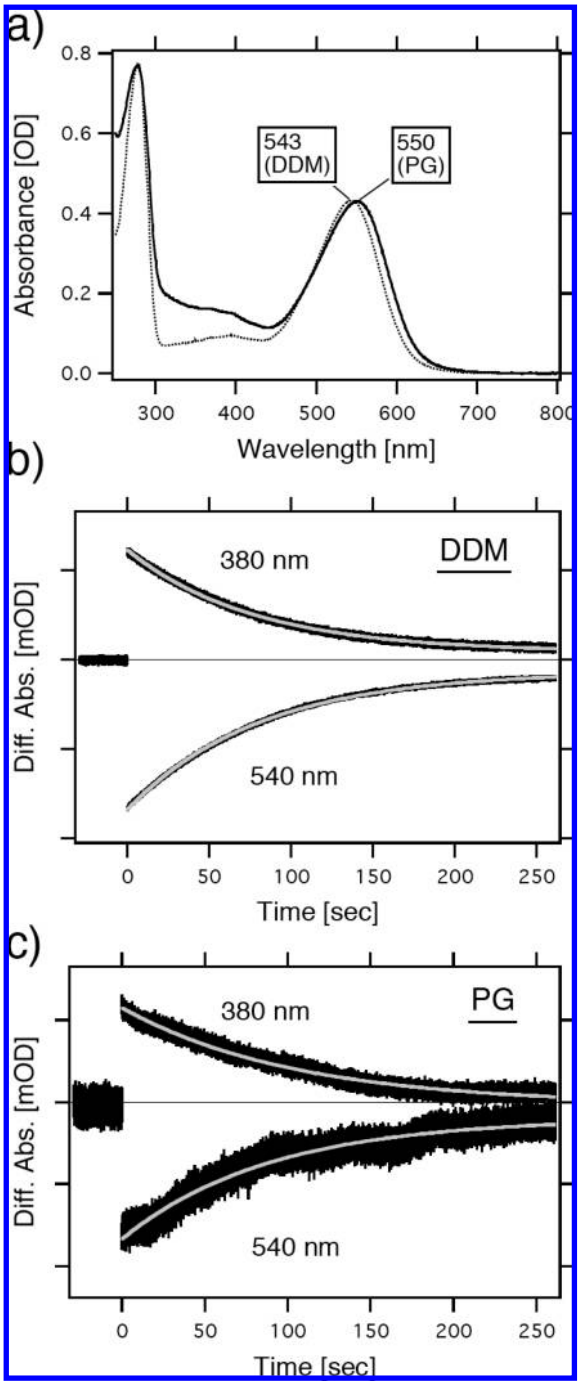

FIGURE 8: (a) Absorption spectra of *Sr*SRI−*Sr*HtrI(1−128) in the DDM micelles or PG liposomes, which have absorption maxima of 543 and 550 nm, respectively. The spectra were measured in a buffer [50 mM Tris-HCl (pH 7.0)] containing 1 M NaCl with 0.1% DDM (DDM) or without DDM (PG). (b) Flash-induced kinetic data of *Sr*SRI−*Sr*HtrI(1−128) in DDM micelles at 380 nm representing the M decay and at 540 nm representing the recovery of the original *Sr*SRI−*Sr*HtrI(1−128) form. The data fit well with a single-exponential decay equation (gray line). (c) Flash-induced kinetic data of *Sr*SRI-*Sr*HtrI(1−128) in the PG liposomes at 380 and 540 nm. The data fit well with a single-exponential decay equation (gray line). One division of the *y*-axis of panels b and c corresponds to 50 and 30 mOD units, respectively.

1−2 orders of magnitude slower than the physiological range for swimming cells that have been studied for taxis behavior. Then the photocycle measurements are apparently greatly perturbed compared to what is expected under physiological conditions.

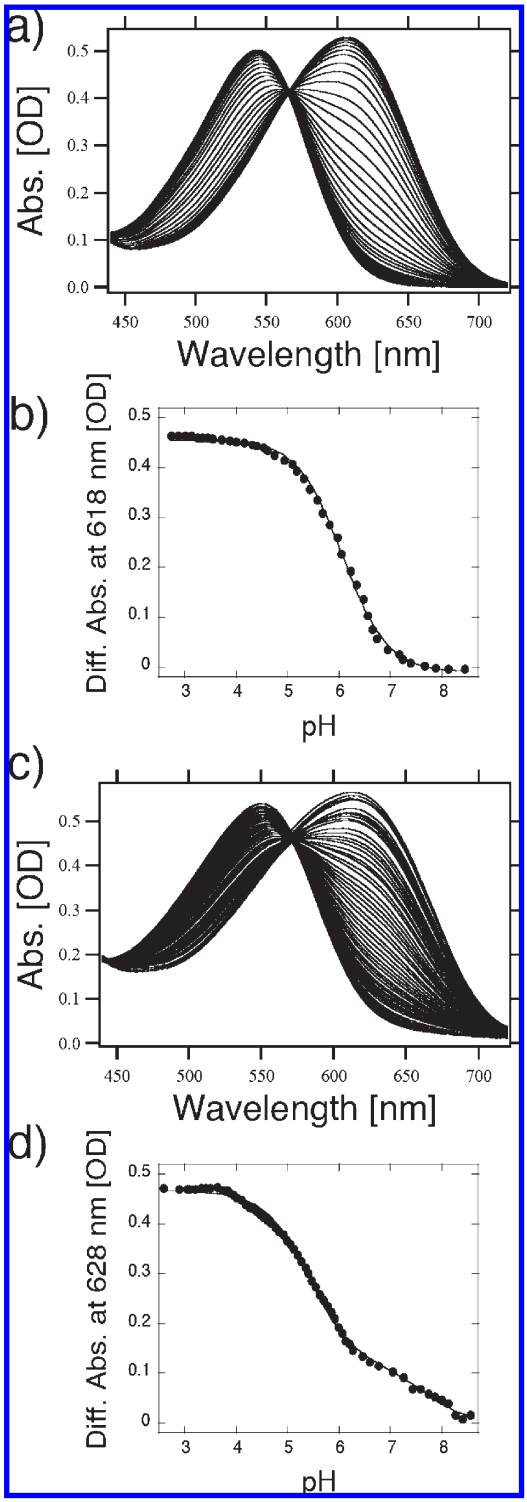

FIGURE 9: (a) Absorption spectra of *Sr*SRI−*Sr*HtrI(1−128) in DDM micelles at varying pH (from 8.46 to 2.75). (b) pH titration curve of the counterion, Asp72, in *Sr*SRI−*Sr*HtrI(1−128). The sample was suspended in a mixture of six buffers with 1 M NaCl. The titration curve was analyzed using the Henderson−Hasselbalch equation with a single pK_a value. The temperature was kept at 20 °C. (c) Absorption spectra of *Sr*SRI−*Sr*HtrI(1−128) in the PG liposomes at varying pH (from 8.56 to 2.6). (d) pH titration curve of the counterion, Asp72, in *Sr*SRI−*Sr*HtrI(1−128). The sample was suspended in a mixture of six buffers with 1 M NaCl. The titration curve was analyzed using the Henderson−Hasselbalch equation with two pK_a values. The temperature was kept at 20 °C. It should be noted that the titration curves presented here were reversible.

Using the *Sr*SRI−*Sr*HtrI(1−128) complex, a spectroscopic pH titration was performed to estimate the pK_a value of Asp72

(Figure 9). The measurements were taken in a buffer containing 1 M NaCl and 0.1% DDM for the solubilized sample (Figure 9a,b) and in a buffer containing 1 M NaCl for the reconstituted sample (Figure 9c,d). The experiments were fit well to the Henderson−Hasselbach equation (*33*) with a single pK_a (Figure 9b) or two pK_a values (Figure 9d), and the pK_a values of Asp72 for *Sr*SRI−*Sr*HtrI(1−128) were estimated to be 6.0 for the DDM-solubilized state and 5.5/7.7 for the PG-reconstituted state. His, Arg, and Lys residue(s) of *Sr*SRI or *Sr*HtrI may be involved in a newly estimated pK_a value (7.7). In any case, the pK_a value of Asp72 is elevated upon *Sr*HtrI association (4.3 → 4.9, 6.0, and 5.5/7.7), although the shift value depends on the sample condition. The molecular mechanism of the effects of the lipids on *Sr*SRI−*Sr*HtrI will be analyzed in the future.

In conclusion, we succeeded in expressing full-length *Sr*HtrI as a fusion protein with *Sr*SRI. *Sr*HtrI altered the photochemical properties of *Sr*SRI, indicating interactions between them. In addition, we identified the photoreactions during the photocycle and compared them to that of *Sr*SRI alone.

ACKNOWLEDGMENT

We thank Dr. Tomomi Kitajima-Ihara for her encouragement.

REFERENCES

1. Spudich, J. L. (2006) The multitalented microbial sensory rhodopsins. *Trends Microbiol. 14*, 480–487.
2. Spudich, J. L., and Bogomolni, R. A. (1984) Mechanism of colour discrimination by a bacterial sensory rhodopsin. *Nature 312*, 509–513.
3. Hoff, W. D., Jung, K. H., and Spudich, J. L. (1997) Molecular mechanism of photosignaling by archaeal sensory rhodopsins. *Annu. Rev. Biophys. Biomol. Struct. 26*, 223–258.
4. Sudo, Y., Kandori, H., and Kamo, N. (2004) Molecular mechanism of protein-protein interaction of *pharaonis* phoborhodopsin/transducer and photo-signal transfer reaction by the complex. *Recent Res. Dev. Biol. 3*, 1–16.
5. Shimono, K., Hayashi, T., Ikeura, Y., Sudo, Y., Iwamoto, M., and Kamo, N. (2003) Importance of the broad regional interaction for spectral tuning in *Natronobacterium pharaonis* phoborhodopsin (sensory rhodopsin II). *J. Biol. Chem. 278*, 23882–23889.
6. Yan, B., Takahashi, T., Johnson, R., Derguini, F., Nakanishi, K., and Spudich, J. L. (1990) All-trans/13-cis isomerization of retinal is required for phototaxis signaling by sensory rhodopsins in *Halobacterium halobium*. *Biophys. J. 57*, 807–814.
7. Kandori, H., Tomioka, H., and Sasabe, H. (2002) Excited-state dynamics of *pharaonis* phoborhodopsin probed by femtosecond fluorescence spectroscopy. *J. Phys. Chem. A 106*, 2091–2095.
8. Chizhov, I., Schmies, G., Seidel, R., Sydor, J. R., Luttenberg, B., and Engelhard, M. (1998) The photophobic receptor from *Natronobacterium pharaonis*: Temperature and pH dependencies of the photocycle of sensory rhodopsin II. *Biophys. J. 75*, 999–1009.
9. Chen, X., and Spudich, J. L. (2002) Demonstration of 2:2 stoichiometry in the functional SRI-HtrI signaling complex in *Halobacterium* membranes by gene fusion analysis. *Biochemistry 41*, 3891–3896.
10. Gordeliy, V. I., Labahn, J., Moukhametzianov, R., Efremov, R., Granzin, J., Schlesinger, R., Buldt, G., Savopol, T., Scheidig, A. J., Klare, J. P., and Engelhard, M. (2002) Molecular basis of transmembrane signalling by sensory rhodopsin II-transducer complex. *Nature 419*, 484–487.
11. Falke, J. J., Bass, R. B., Butler, S. L., Chervitz, S. A., and Danielson, M. A. (1997) The two-component signaling pathway of bacterial chemotaxis: A molecular view of signal transduction by receptors, kinases, and adaptation enzymes. *Annu. Rev. Cell Dev. Biol. 13*, 457–512.
12. Rudolph, J., and Oesterhelt, D. (1996) Deletion analysis of the che operon in the archaeon *Halobacterium salinarium*. *J. Mol. Biol. 258*, 548–554.
13. Trivedi, V. D., and Spudich, J. L. (2003) Photostimulation of a sensory rhodopsin II/HtrII/Tsr fusion chimera activates CheA-autophosphorylation and CheY-phosphotransfer in vitro. *Biochemistry 42*, 13887–13892.
14. Sudo, Y., Yamabi, M., Kato, S., Hasegawa, C., Iwamoto, M., Shimono, K., and Kamo, N. (2006) Importance of specific hydrogen bonds of archaeal rhodopsins for the binding to the transducer protein. *J. Mol. Biol. 357*, 1274–1282.
15. Sudo, Y., Furutani, Y., Kandori, H., and Spudich, J. L. (2006) Functional importance of the interhelical hydrogen bond between Thr204 and Tyr174 of sensory rhodopsin II and its alteration during the signaling process. *J. Biol. Chem. 281*, 34239–34245.
16. Sudo, Y., Yamabi, M., Iwamoto, M., Shimono, K., and Kamo, N. (2003) Interaction of *Natronobacterium pharaonis* phoborhodopsin (sensory rhodopsin II) with its cognate transducer probed by increase in the thermal stability. *Photochem. Photobiol. 78*, 511–516.
17. Shimono, K., Iwamoto, M., Sumi, M., and Kamo, N. (1997) Functional expression of pharaonis phoborhodopsin in *Escherichia coli*. *FEBS Lett. 420*, 54–56.
18. Sudo, Y., Iwamoto, M., Shimono, K., and Kamo, N. (2001) Pharaonis phoborhodopsin binds to its cognate truncated transducer even in the presence of a detergent with a 1:1 stoichiometry. *Photochem. Photobiol. 74*, 489–494.
19. Sasaki, J., and Spudich, J. L. (2008) Signal transfer in Haloarchaeal sensory rhodopsin−transducer complexes. *Photochem. Photobiol. 84*, 863–868.
20. Mironova, O. S., Budyak, I. L., Büldt, G., Schlesinger, R., and Heberle, J. (2007) FT-IR difference spectroscopy elucidates crucial interactions of sensory rhodopsin I with the cognate transducer HtrI. *Biochemistry 46*, 9399–9405.
21. Kim, Y. J., Chizhov, I., and Engelhard, M. (2009) Functional expression of the signaling complex sensory rhodopsin II/transducer II from *Halobacterium salinarum* in *Escherichia coli*. *Photochem. Photobiol. 85*, 521–528.
22. Mongodin, E. F., Nelson, K. E., Daugherty, S., Deboy, R. T., Wister, J., Khouri, H., Weidman, J., Walsh, D. A., Papke, R. T., Sanchez Perez, G., Sharma, A. K., Nesbo, C. L., MacLeod, D., Bapteste, E., Doolittle, W. F., Charlebois, R. L., Legault, B., and Rodriguez-Valera, F. (2005) The genome of *Salinibacter ruber*: Convergence and gene exchange among hyperhalophilic bacteria and archaea. *Proc. Natl. Acad. Sci. U.S.A. 102*, 18147–18152.
23. Kitajima-Ihara, T., Furutani, Y., Suzuki, D., Ihara, K., Kandori, H., Homma, M., and Sudo, Y. (2008) *Salinibacter* sensory rhodopsin: sensory rhodopsin I-like protein from a eubacterium. *J. Biol. Chem. 283*, 23533–23541.
24. Marmur, J. (1961) A procedure for the isolation of DNA from microorganisms. *J. Mol. Biol. 3*, 208–218.
25. Suzuki, D., Furutani, Y., Inoue, K., Kikukawa, T., Sakai, M., Fujii, M., Kandori, H., Homma, M., and Sudo, Y. (2009) Effects of chloride ion binding on the photochemical properties of *Salinibacter* sensory rhodopsin I. *J. Mol. Biol. 392*, 48–62.
26. Balashov, S. P., Imasheva, E. S., Boichenko, V. A., Anton, J., Wang, J. M., and Lanyi, J. K. (2005) Xanthorhodopsin: A proton pump with a light-harvesting carotenoid antenna. *Science 309*, 2061–2064.
27. Jung, K. H., and Spudich, J. L. (1998) Suppressor mutation analysis of the sensory rhodopsin I-transducer complex: Insights into the color-sensing mechanism. *J. Bacteriol. 180*, 2033–2042.
28. Zhang, X. N., Zhu, J., and Spudich, J. L. (1999) The specificity of interaction of archaeal transducers with their cognate sensory rhodopsins is determined by their transmembrane helices. *Proc. Natl. Acad. Sci. U.S.A. 96*, 857–862.
29. Sasaki, J., Nara, T., Spudich, E. N., and Spudich, J. L. (2007) Constitutive activity in chimeras and deletions localize sensory rhodopsin II/HtrII signal relay to the membrane-inserted domain. *Mol. Microbiol. 66*, 1321–1330.
30. Sudo, Y., and Spudich, J. L. (2006) Three strategically placed hydrogen-bonding residues convert a proton pump into a sensory receptor. *Proc. Natl. Acad. Sci. U.S.A. 103*, 16129–16134.
31. Haupts, U., Tittor, J., and Oesterhelt, D. (1999) Closing in on bacteriorhodopsin: Progress in understanding the molecule. *Annu. Rev. Biophys. Biomol. Struct. 28*, 367–399.
32. Spudich, J. L. (1995) Transducer protein HtrI controls proton movements in sensory rhodopsin I. *Biophys. Chem. 56*, 165–169.
33. Sudo, Y., Iwamoto, M., Shimono, K., and Kamo, N. (2002) Tyr-199 and charged residues of pharaonis phoborhodopsin are important for the interaction with its transducer. *Biophys. J. 83*, 427–432.
34. Swartz, T. E., Szundi, I., Spudich, J. L., and Bogomolni, R. A. (2000) New photointermediates in the two photon signaling pathway of sensory rhodopsin-I. *Biochemistry 39*, 15101–15109.
35. Chizov, I., Schmies, G., Seidel, R., Sydor, J. R., Lüttenberg, B., and Engelhard, M. (1999) The photophobic receptor from *Natronobacterium pharaonis*: Temperature and pH dependencies of the photocycle of sensory rhodopsin II. *Biophys. J. 75*, 999–1009.

36. Spudich, J. L., and Lanyi, J. K. (1996) Shuttling between two protein conformations: The common mechanism for sensory transduction and ion transport. *Curr. Opin. Cell Biol. 8*, 452–457.
37. Lanyi, J. K., and Luecke, H. (2001) Bacteriorhodopsin. *Curr. Opin. Struct. Biol. 11*, 415–419.
38. Spudich, J. L., Yang, C. S., Jung, K. H., and Spudich, E. N. (2000) Retinylidene proteins: Structures and functions from archaea to humans. *Annu. Rev. Cell Dev. Biol. 16*, 365–392.
39. Spudich, E. N., and Spudich, J. L. (1993) The photochemical reactions of sensory rhodopsin I are altered by its transducer. *J. Biol. Chem. 268*, 16095–16097.
40. Bogomolni, R. A., and Spudich, J. L. (1987) The photochemical reactions of bacterial sensory rhodopsin-I. Flash photolysis study in the one microsecond to eight second time window. *Biophys. J. 52*, 1071–1075.
41. Sudo, Y., Iwamoto, M., Shimono, K., and Kamo, N. (2004) Role of charged residues of pharaonis phoborhodopsin (sensory rhodopsin II) in its interaction with the transducer protein. *Biochemistry 43*, 13748–13754.
42. Bergo, V. B., Spudich, E. N., Rothschild, K. L., and Spudich, J. L. (2005) Photoactivation perturbs the membrane-embedded contacts between sensory rhodopsin II and its transducer. *J. Biol. Chem. 280*, 28365–28369.
43. Furutani, Y., Kamada, K., Sudo, Y., Shimono, K., Kamo, N., and Kandori, H. (2005) Structural changes of the complex between *pharaonis* phoborhodopsin and its cognate transducer upon formation of the M photointermediate. *Biochemistry 44*, 2909–2915.
44. Shimono, K., Ikeura, Y., Sudo, Y., Iwamoto, M., and Kamo, N. (2001) Environment around the chromophore in pharaonis phoborhodopsin: Mutation analysis of the retinal binding site. *Biochim. Biophys. Acta 1515*, 92–100.
45. Sudo, Y., Iwamoto, M., Shimono, K., and Kamo, N. (2002) Association of pharaonis phoborhodopsin with its cognate transducer decreases the photo-dependent reactivity by water-soluble reagents of azide and hydroxylamine. *Biochim. Biophys. Acta 1558*, 63–69.
46. Sudo, Y., Okuda, H., Yamabi, M., Fukuzaki, Y., Mishima, M., Kamo, N., and Kojima, C. (2005) Linker region of a halobacterial transducer protein interacts directly with its sensor retinal protein. *Biochemistry 44*, 6144–6152.
47. Taylor, B. L. (2007) Aer on the inside looking out: Paradigm for a PAS-HAMP role in sensing oxygen, redox and energy. *Mol. Microbiol. 65*, 1415–1424.